Textile Science & Research Journal
ISSN: 3059-846X, Volume – 2, Issue – 2, 2026
DOI: https://doi.org/10.63456/tsrj-2-2-46

DISTRIBUTION OF COMPACTION PRESSURE IN FABRIC REINFORCEMENT STACKS DURING COMPOSITES MANUFACTURING

[1]SIMON BARIL-GOSSELIN, [2]FRANCOIS ROBITAILLE

[1]Automotive and Surface Transportation Research Centre, National Research Council Canada, Canada, Simon.Baril-Gosselin@cnrc-nrc.gc.ca

[2] Department of Mechanical Engineering, University of Ottawa, Canada, Francois.robitaille@uottawa.ca

Francois Robitaille: Francois.robitaille@uottawa.ca

Corresponding author: FRANCOIS ROBITAILLE

ABSTRACT

Through-thickness compaction of fabric reinforcements plays a central role in the manufacturing and performance of polymer-matrix composites (PMCs) as it governs fibre volume fraction (v_f) and fabric permeability. Theoretical models describing the effect of fabric architecture on the spatial distribution of compaction pressure are available, yet direct experimental evidence of pressure heterogeneity in compacted stacks of textiles remains scarce. In this work, distributions of compaction pressures measured at different locations within stacks of woven and non-crimp (NCF) carbon fibre reinforcement fabrics are reported for different fabric architectures, surface densities and cover factors. Local compaction pressures were measured using calibrated pressure measurement films interleaved between fabric plies. Measurements were performed in situ under 1 bar vacuum at multiple locations within the stacks, including against the moulding tool and bagging material, and for different relative ply orientations. Two configurations representative of composite manufacturing were investigated: dry reinforcement stacks and stacks of fabric plies interleaved with uncured epoxy resin films. Compaction pressure distributions were consistently heterogeneous and exhibited repeating patterns traceable to fabric architecture. In dry reinforcement stacks, zones of high pressure (>0.5 bar) covered on average 30 % to 45 % of the surface area depending on fabric architecture and ply orientation. When resin films were present, high-pressure zones increased to approximately 50 % to 60 % of the surface area and pressure transitions became more gradual. No clear correlation was found between the extent of compaction pressure zones and macroscopic fabric descriptors such as fibre volume fraction v_f, fabric surface density or initial fabric cover factor. However, pressure distribution could be explained using a more detailed description of the fabric topography. Results demonstrate that local fabric architecture dominates pressure distribution during compaction and highlight the need to account for mesoscale pressure heterogeneity in composite manufacturing models to improve control and consistency of part quality.

KEYWORDS: Carbon fibre fabrics, Compaction pressure, Distribution, Heterogeneity, Measurement, Composite

1. INTRODUCTION AND LITERATURE

Through-thickness compaction of fabric reinforcements normal to their plane plays a central role in the manufacturing and performance of polymer composite materials (PMCs) made from such reinforcements. To be competitive as high-performance structural materials, PMCs must reach high fibre volume fractions (v_f) that can only be achieved through normal compaction of the fabric reinforcements. Some PMC manufacturing processes such as vacuum-assisted resin transfer moulding (VARTM) start with the compaction of stacks of dry fabric plies only. However, in other processes such as resin film infusion (RFI), fabric reinforcements are interleaved with films of uncured resin prior to compaction, and subsequent local flow and saturation of the reinforcements by hot melt resin are entirely driven by local, normal compaction pressure. Therefore, understanding local compaction pressure and its distribution in compacted stacks of reinforcement fabrics, dry and interleaved, is critical to the manufacturing and to the performance of PMCs [1-12].

Given its importance, the compaction behaviour of fabric reinforcement stacks normal to their plane was quantified experimentally and it was modelled; review papers and international benchmarking exercises are noted [13-15]. Most published experimental results are reported as curves relating single average values of applied compaction pressure to macroscopic values of stack v_f or thickness. As such, the compaction behaviour is typically quantified as if fabrics were homogeneous and continuous media, even as fabric architectures are mentioned systematically in publications. Such experimental data do not describe distributions of compaction pressure, nor enable sound understanding of the compaction of reinforcement fabric stacks. The open literature features only very limited experimental evidence or description of the heterogeneity and distribution of compaction pressure within fabric stacks, or of the effects of fabric architecture and stacking sequences on pressure distribution. Similarly, published results do not document differences in pressure distributions near hard tooling, soft tooling ancillaries or uncured resin films, even as macroscopic compaction behaviour is known to change in the presence of a second phase in the stack or as a function of fabric architecture and cover factor [10, 11]. Different levels of nesting are known to lead to variability in compaction behaviour and other properties at unit cell

scale [16, 17]. The effects of fabric architecture and pressure heterogeneity at unit cell scale can be observed at the macroscopic scale: yarn reorganisation is clearly visible after compaction [12] and under other load cases [18].

Efforts were devoted to instrumenting fabric stacks towards direct in-situ measurement, with most work aimed at monitoring local resin flow [19-21]. Ali et al. [22] reported work aiming at enabling better understanding of fabric compaction in the form of a coated fabric sensor enabling in-situ measurements of pressure. The work shows much promise; however, results reported still describe pressure as single average values for the entire surface of fabrics.

Analytical and computational models of fabric compaction were proposed. Different authors [6, 16, 23-26] accounted for fabric architecture by including constitutive, rheological or other empirical elements associated with different elements of the fabric or their different scales, or they modelled fabric architecture explicitly in computational meshes. However, results do not describe the distribution of local compaction pressure or its heterogeneity; here again, pressure is represented as average values.

This paper presents distributions of compaction pressure measured directly at different locations within stacks of 8 plies of woven and non-crimp (NCF) carbon fibre reinforcement fabrics for different fabric architectures, surface densities and cover factors. Two primary series of tests were conducted. Series 1 tests were performed on stacks of fabric plies only. Series 2 tests were performed on stacks where all fabric plies were interleaved with films of uncured epoxy resin. Each series replicated different PMC manufacturing processes. In both Series 1 and Series 2, stacks were compacted under 1.0 bar nominal pressure between a platen on one side and peel ply, breather plies and a vacuum film on the other side. Distributions of local compaction pressure at different positions within the stacks were obtained using image analysis of patterns imprinted on calibrated pressure measurement films interleaved between plies, within the stacks. The patterns were analysed qualitatively and quantitatively. Pressure distributions were measured in-situ at 5 locations: A) next to hard tooling surfaces, B) next to soft tooling surfaces, and between fabric plies featuring C) parallel yarns and/or stitch lines, D) perpendicular yarns and/or stitch lines, and E) yarns and/or stitch lines separated by 45°, on their opposing faces. Heterogeneity and patterns in pressure distributions appeared clearly in all cases.

2 MATERIALS AND METHODS

2.1 FABRICS AND COVER FACTORS

Four carbon fibre fabrics with different surface densities and architectures were used for assessing pressure distribution in compacted stacks: 1) 197 g/m^2 (0°/90°) plain weave PW-L made by Texonic from 3K yarns; 2) 429 g/m^2 (0°/90°) 2×2 twill weave Twill-H made by Texonic from 6K yarns; 3) 250 g/m^2 (-45°/+45°) bidirectional non-crimp tricot stitched fabric NCF-L made by Saertex from 12K yarns; and 4) 534 g/m^2 (-45°/+45°) bidirectional non-crimp chain stitched fabric NCF-H made by Saertex from 12K yarns. Letters L and H indicate fabrics of lower and higher surface densities hence the selection included all four combinations of weaves or NCF fabrics, each with lower or higher surface densities. All fabrics featured Teijin Tenax HTS 40 carbon fibres. Supplier stated and measured surface densities, measured yarn width w_y and measured yarn spacing d_s appear in Table 1 along with measured spacing between neighbouring crossovers for weaves and between parallel stitch lines for NCFs. Photographs of the fabrics appear in Figure 1.

Values of linear cover factors CF_{warp} and CF_{weft} and total cover factor CF for fabrics as-received and after compaction to 1.0 bar nominal pressure appear in Table 2. Linear cover factors CF_{warp} and CF_{weft} are the proportions of projected area covered by either warp or weft yarns; they can take different values along both directions. The total cover factor CF is the proportion of projected area covered by either or both warp and/or weft yarns. All values of CF_{warp}, CF_{weft} and CF are indicative of the heterogeneity of fabric architecture as they quantify the relative size of inter-yarn gaps. Values were obtained from analysis of optical microscopy images. The linear cover factor CF_x is equal to:

$$CF_x = \frac{w_y}{d_s} \quad (1)$$

where measured yarn spacing d_s represents the distance between one edge of a yarn and the same edge on the neighbouring yarn, and yarn width w_y is self-explanatory; therefore, $d_s > w_y$ and $CFx < 1$. The total cover factor CF is equal to:

$$CF = CF_{warp} + CF_{weft} - CF_{warp} \times CF_{weft} \quad (2)$$

All values were averaged from five distinct photographs with each geometric parameter listed in Tables 1 and 2 quantified from at least 30 measurements. Fabrics Twill-H, NCF-L and NCL-H showed higher values of CF_{warp}, CF_{weft} and CF, the latter being similar for these three fabrics, while fabric PW-L featured larger gaps between yarns. Linear cover factors were largely independent of orientation for fabrics PW-L, NCF-L and NCF-H while fabric Twill-H featured a greater linear cover factor in the warp direction.

Textile Science & Research Journal
ISSN: 3059-846X, Volume – 2, Issue – 2, 2026
DOI: https://doi.org/10.63456/tsrj-2-2-46

Table 1: Supplier stated and measured surface densities, yarn width w_y , yarn spacing d_s and crossover/stitch line spacing for fabrics PW-L, Twill-H, NCF-L and NCF-H

Fabric	Surface density, stated (g/m^2)	Surface density, measured (g/m^2)	w_y Yarn width (mm)	d_s Yarn spacing (mm)	Crossover or Stitch line spacing (mm)
PW-L	197	192.4 ± 5.4	1.55 ± 0.10	2.11 ± 0.11	2.11 ± 0.22
Twill-H	429	403.2 ± 3.5	1.89 ± 0.16	2.01 ± 0.15	4.02 ± 0.21
NCF-L	250	254.1 ± 4.6	1.70 ± 0.19	1.81 ± 0.20	7.34 ± 0.08
NCF-H	534	537.8 ± 5.9	1.60 ± 0.15	1.76 ± 0.16	7.04 ± 0.22

Table 2: Linear cover factors CF_{warp} and CF_{weft} , and total cover factor CF for fabrics PW-L, Twill-H, NCF-L and NCF-H as-received and after compaction to 1.0 bar nominal pressure

Fabric	CF_{warp} as received	CF_{weft} as received	CF as received	CF 1.0 bar
PW-L	0.728 ± 0.045	0.738 ± 0.067	0.928	0.943
Twill-H	0.978 ± 0.035	0.899 ± 0.058	0.998	1.000
NCF-L	0.939 ± 0.042	0.935 ± 0.055	0.996	0.995
NCF-H	0.911 ± 0.047	0.912 ± 0.058	0.992	0.998

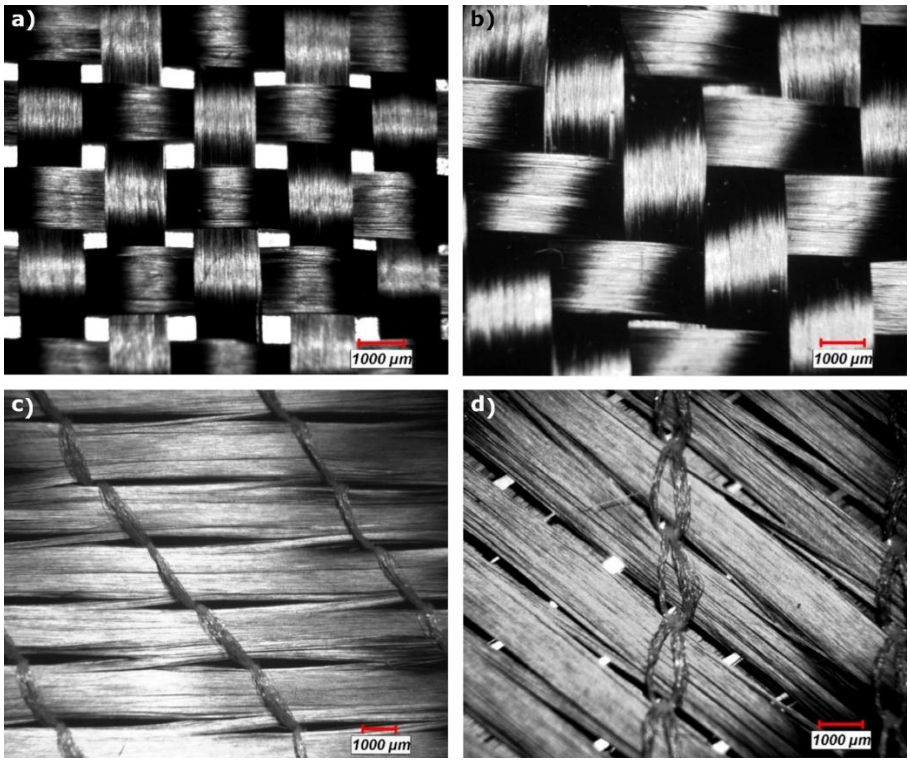

Figure 1: Photographs of fabrics; a) PW-L, b) Twill-H, c) NCF-L, d) NCF H

2.2 CHARACTERISATION OF FABRIC REORGANISATION

Limited increases in cover factor under nominal compaction pressure of 1.0 bar were generally observed as shown in Table 2. Such increases result from reorganisation of the fabric architecture taking place during compaction, primarily through yarn flattening and widening, leading to reinforcement stacks with lower thickness and increased fibre volume fraction v_f [13]. The capacity for reorganisation of a reinforcement fabric is indicative of its behaviour under normal compaction. Therefore, as part of initial fabric characterisation prior to test Series 1 and Series 2, reorganisation was assessed by compacting samples between 150 mm diameter rigid platens to 10.0 bar at a rate of 0.5 mm/min using an Instron 4482 load

Textile Science & Research Journal
ISSN: 3059-846X, Volume – 2, Issue – 2, 2026
DOI: https://doi.org/10.63456/tsrj-2-2-46

frame equipped with a 100 kN load cell; 50 successive compaction cycles were performed on stacks of all four fabrics. Average fibre volume fraction v_f was quantified through cross-head motion with previously measured load frame deformation subtracted from cross-head motion data. Stack thickness t_{stack} was converted to v_f as the ratio of the volume of fibres V_{fabric} to volume between the platens V_{stack} :

$$v_f = \frac{V_{fabric}}{V_{stack}} = \frac{\left(A \frac{N_{plies}\,\rho_s}{\rho_{fibre}}\right)}{(A\,t_{stack})} = \frac{N_{plies}\,\rho_s}{\rho_{fibre}\,t_{stack}} \quad (3)$$

where A is the compaction surface, N_{plies} is the number of fabric plies, ρ_s is the surface density of a single fabric ply and ρ_{fibre} is the density of the fibres. Multiple trials showed that v_f deviated by less than ± 1% between repeats. Results in Table 3 show that reorganisation occurred in all fabrics. Both fabrics with higher surface density reached higher maximum v_f . Considering L and H surface densities separately, in both cases the NCF fabric reached lower maximum v_f than the corresponding weave, possibly due to the presence of stitch lines. No clear relationship between maximum v_f and cover factor was observed.

Table 3: Fabric fibre volume fraction v_f after 1 and 50 compaction cycles to 10.0 bar for fabrics PW-L, Twill-H, NCF-L and NCF-H, along with original values under 1.0 bar

Compaction cycle (#)	PW-L	Twill-H	NCF-L	NCF-H
	Fabric fibre volume fraction v_f (%) under 10.0 bar			
1	66.8	71.3	63.4	70.7
50	73.5	76.2	67.9	75.0
	Fabric fibre volume fraction v_f (%) under 1.0 bar			
1	55.7	59.7	51.1	58.7

2.3 STACKING SEQUENCES

Compaction tests Series 1 and Series 2 to 1.0 bar nominal pressure applied under vacuum, as well as the aforementioned fabric reorganisation characterisation trials to 10.0 bar compaction pressure applied between platens, were all performed on 8-layer fabric stacks with stacking sequences listed in Table 4. The symmetric sequences featured all different possible cases of yarns parallel, perpendicular and separated by 45° on opposite faces of neighbouring plies, for quasi-isotropic laminates made from balanced bidirectional fabrics. NCF fabrics showed different stitch patterns on their top and bottom sides; the stacking sequences enabled all possible combinations of the same sides (top-top and bottom-bottom) or opposite sides (top-bottom) being in direct contact with yarns parallel, perpendicular and separated by 45° on opposite faces of neighbouring plies.

Samples used were significantly larger than textile repeating unit cells for all fabrics tested, and stacks featured 8 plies. Therefore, no specific efforts were made for aligning yarns for either maximum or minimum nesting. Orientations were well controlled but relative translations along the warp or weft were not. Such artificial alignment can be useful in analytical models featuring a limited number of unit cells and plies, but it is not representative of industrial reality in experimental characterisation work. It is interesting to note that clear repeating pattens appeared in pressure distributions despite specific translational alignment along the warp or weft, as shown in following sections.

Table 4: Stacking sequences for compacted fabrics PW-L, Twill-H, NCF-L and NCF-H

Fabric	PW-L , Twill-H	NCF-L	NCF-H
Stacking	$[(0/90)_3, (+45/-45)]_S$	$[(0/90), (90/0)_2 (+45/-45)]_S$	$[(0/90), (90/0)_2 (+45/-45)]_S$
Layer #1	(0/90)	$(0^T/90^B)$	$(0^B/90^T)$
Layer #2	(0/90)	$(90^T/0^B)$	$(90^B/0^T)$
Layer #3	(0/90)	$(90^T/0^B)$	$(90^B/0^T)$
Layer #4	(+45/-45)	$(+45^B/-45^T)$	$(+45^B/-45^T)$
Layer #5	(-45/+45)	$(-45^T/+45^B)$	$(-45^T/+45^B)$
Layer #6	(90/0)	$(0^T/90^B)$	$(0^B/90^T)$
Layer #7	(90/0)	$(0^B/90^T)$	$(0^T/90^B)$
Layer #8	(90/0)	$(90^T/0^B)$	$(90^T/0^B)$

Notes: - (θ_1/θ_2) denotes bidirectional fabric orientation where θ_1 and θ_2 are warp and weft yarns respectively

- Superscripts T and B represent top and bottom sides of the fabric as determined by stitching pattern

Textile Science & Research Journal
ISSN: 3059-846X, Volume – 2, Issue – 2, 2026
DOI: https://doi.org/10.63456/tsrj-2-2-46

2.4 INTERLEAVED RESIN FILM

Compaction test Series 1 and Series 2 trials to 1.0 bar nominal pressure applied under vacuum both characterised the distribution of compaction pressure at positions A to E within stacks. Series 1 characterised pressure distributions within stacks of dry fabric plies only, documenting interactions between opposing yarns and stitch lines in configurations representative of PMC manufacturing processes such as VARTM. Series 2 documented interactions between fabric plies interleaved with uncured resin films, in configurations representative of PMC manufacturing processes such as RFI. The 150 g/m^2 resin film used in Series 2 was epoxy-based resin film SA 70 supplied by Gurit with glass transition temperature T_g = 120°C; all compaction tests were conducted at room temperature. All stacks in both Series 1 and Series 2 tests featured 8 carbon fibre fabric plies; in all Series 2 tests, one resin film ply was interleaved between all pairs of fabric plies.

2.5 APPARATUS AND PRESSURE FILM

Test Series 1 and Series 2 characterised the distribution of compaction pressure in stacks of dry reinforcement fabrics and in stacks of reinforcement fabrics interleaved with resin films respectively. All Series 1 and Series 2 tests were conducted under -0.98 bar vacuum (1.0 bar nominal pressure) applied for 120 seconds. All stacks were covered with 1 ply of release film Wrightlon 5200B, 2 plies of breather material UltraWeave 606 and 1 ply of Securlon L-1000 bagging film, all from Airtech, sealed over a 15 mm glass platen covered with 1 ply of release film, Figure 2. All stacks were interleaved with 50 mm by 25 mm Fujifilm Prescale extreme low pressure measurement film featuring a colour-developing sheet and micro-encapsulated red coloured material with 0.5 bar bursting pressure. Compaction pressure distribution was assessed at five locations labelled A to E within fabric stacks: A) next to hard tooling surfaces, B) next to soft tooling surfaces, and between fabric plies featuring C) parallel yarns and/or stitch lines, D) perpendicular yarns and/or stitch lines, and E) yarns and/or stitch lines separated by 45°, on their opposing faces. After 120 seconds the bagging and ancillary films were carefully unsealed and removed, and individual pressure measurement films were extracted for analysis. Pressure measurement films were analysed qualitatively for pressure distribution patterns and quantitatively for assessing coverage of high-pressure zones, using image analysis software ImageJ. For qualitative analysis, the films were digitised using a flatbed scanner, ensuring image flatness and colour consistency between scans. Coverage was calculated as the ratio of the number of coloured pixels to the total number of pixels in each image of pressure measurement films. A colour saturation value of 30 out of 255 was used as the cut-off point for all images to define coloured pixels; an example of the segmentation appears in Figure 3. Colour saturation was used for the threshold instead of image brightness to ensure that only the ink of the films would be captured in the analysis.

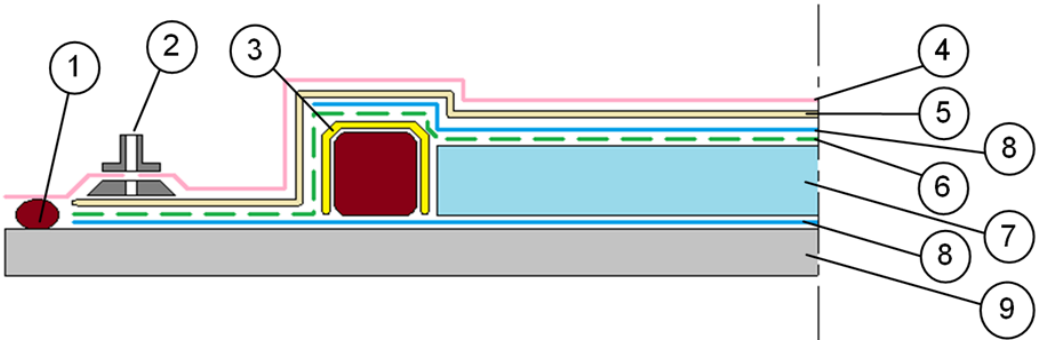

Figure 2: Bagging method; 1) sealant tape; 2) vacuum valve; 3) glass fabric; 4) bag; 5) breather; 6) perforated film; 7) stack; 8) release film; 9) tool

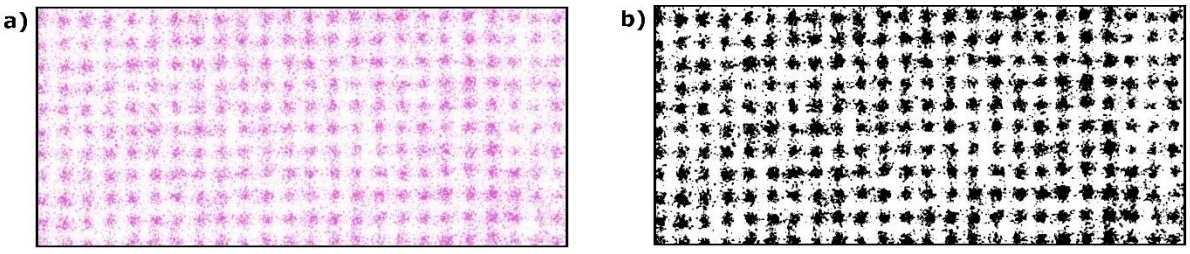

Figure 3: Pressure measurement film; a) after compaction, b) binary image from thresholding

Textile Science & Research Journal
ISSN: 3059-846X, Volume – 2, Issue – 2, 2026
DOI: https://doi.org/10.63456/tsrj-2-2-46

3. RESULTS

3.1 SERIES 1: DISTRIBUTION OF COMPACTION PRESSURE IN STACKS OF FABRIC PLIES ONLY

Pressure distributions at different stack locations tested in Series 1 are presented in Figure 4. Pressure measurement films appear in white in Figure 4, with high-pressure zones where compaction pressure exceeded 0.5 bar appearing in red. All pressure measurement films measured 50.4 mm by 25.4 mm, capturing multiple fabric repeating unit cells. At location A, discrete zones of high pressure are clearly visible for all fabrics in plies next to the platen. For weaves, zones of higher compaction pressure form regular patterns at yarn crossovers where warp and weft yarns overlap, with differences observed in the patterns for the two weaves. Irregular nesting was present on the stack side of both weaves in contact with further plies. However, highly regular patterns observed in Figure 4 for location A show that nesting irregularity further inside the stack did not affect pressure distribution on the platen side for either woven fabrics. For NCFs, zones of higher compaction pressure also appear in regular patterns, primarily in and around sites where stitch lines and yarns superimpose. As a result, patterns show features that can be associated with both yarns and stitch lines.

At location B, pressure distribution patterns in fabrics next to the release film and breather are similar to those observed in fabrics next to the platen, at location A. Similarly to location A, regular patterns observed in Figure 4 for location B show that nesting irregularity further inside the stack did not affect pressure distribution on the bag side for any fabric. However, the presence of conformable release film and breather lead to more uniform pressure distributions as indicated by more progressive fluctuations and coloured dots visible in inter-yarn regions, for all fabrics.

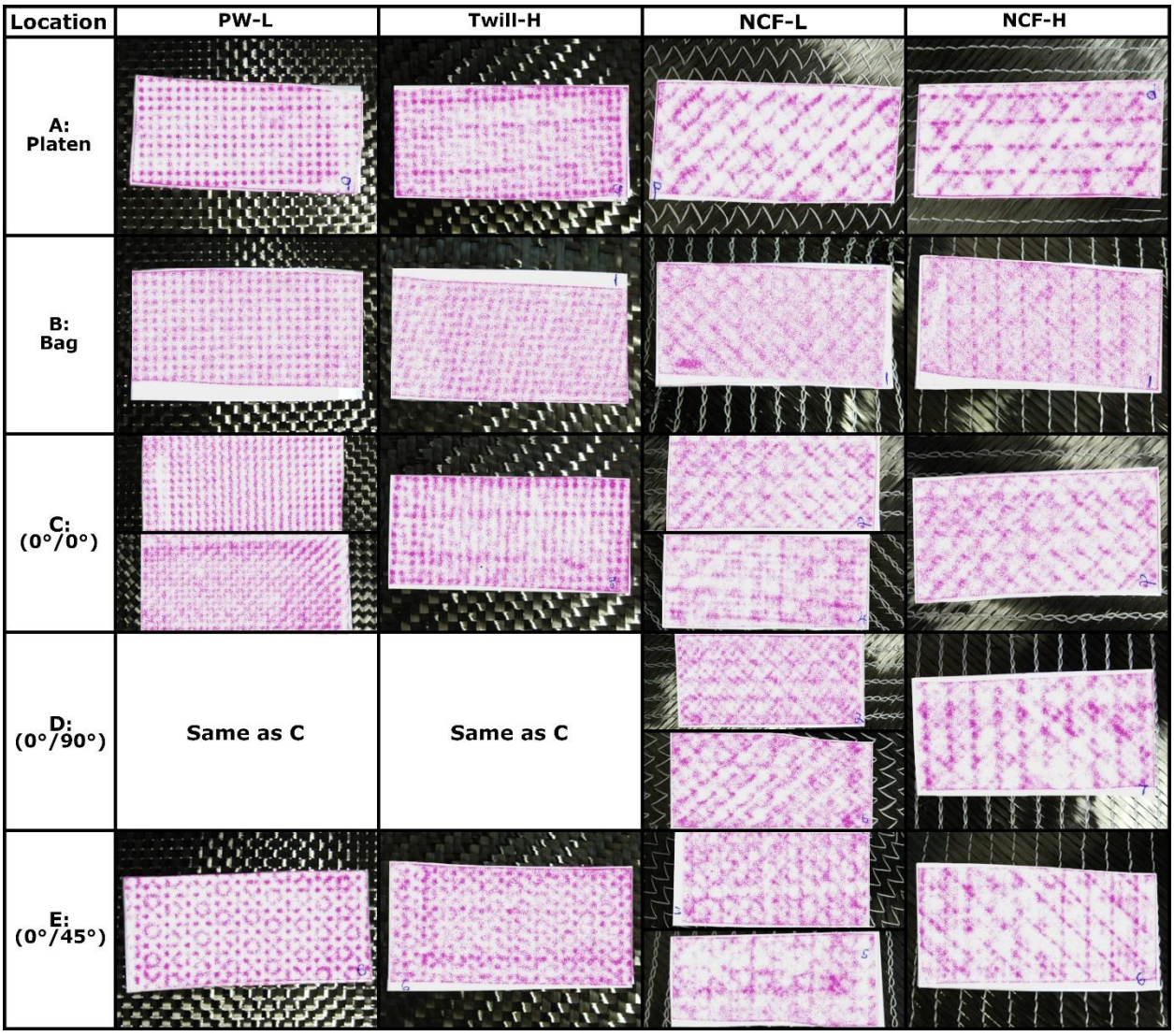

Figure 4: Pressure distribution within stack of PW-L, Twill-H, NCF-L and NCF-H fabrics plies only, at locations A, B, C, D and E within stacks

Textile Science & Research Journal
ISSN: 3059-846X, Volume – 2, Issue – 2, 2026
DOI: https://doi.org/10.63456/tsrj-2-2-46

At location C with contiguous plies and opposing parallel yarns, patterns are more complex than in previous cases because of fabric nesting. For weaves, zones of higher compaction pressure are more visible where contiguous yarns align. Conversely, increased nesting through offset yarns leads to markedly more uniform pressure distributions. Ply alignment has less impact on NCFs because of the prevalent effect of stitch lines. For tricot stitch fabric NCF-L, pressure distributions differ with contacting sides as a result of different stitch patterns on top and bottom sides. Pressure distribution is more uniform for contiguous top and bottom sides, with higher compaction pressures observed at stitch line crossings.

At location D with contiguous plies and perpendicular yarns, symmetry in weaves leads to results identical to those presented above. For NCFs, again pressure distributions were primarily dependent on stitch lines. Pressure distributions in tricot stitched fabric NCF-L with contiguous top and bottom sides were similar to those seen for parallel yarns, suggesting limited yarn impact. This configuration provided the most homogeneous pressure distribution observed in stacks of fabrics only. Contiguous bottom sides resulted in a zigzag pattern following stitch threads, with no yarn orientations visible. Again, yarn orientation had limited effect on pressure distribution for this tricot stitched NCF.

At location E with contiguous fabric plies and opposing yarns at 45° from each other, pressure distributions in weaves show specific cross and circle patterns, notably visible for the plain weave. Pressure distributions in NCFs are governed by stitch lines, similarly to other cases.

The results of quantitative analysis of pressure patterns imprinted on all measurement films tested in Series 1 appear in Figures 5 and 6. All results indicate clear heterogeneity and patterns for zones of high compaction pressure resulting from fabric architecture. Quantitative results for coverage of high compaction pressure zones at different locations within the stacks, for all fabrics tested in Series 1, appear in Figure 5a. Coverage of high compaction pressure zones was marginally greater at interfaces with release film and breather, location B, than at interfaces with the platen, location A, or elsewhere within stacks. When all fabrics were analysed together as a group, differences were visible but not statistically significant.

Coverage of high compaction pressure zones showed more variation between different fabrics and between relative orientations of yarns in contiguous plies, Figure 5b. In this Figure, 0° and 90° both indicate contiguous fabric plies with opposing parallel yarns, and 45° indicates contiguous fabric plies where opposing yarns from an angle of 45°; values for 0° and 90° configurations differ for NCFs as a result of stitch line configurations. Differences are observed between fabrics PW-L and Twill-H; a parallel with their different fabric cover factors *CF* can be drawn. However, no relationship was observed between fabric cover factor and fibre volume fraction, hence it can never be assumed that fabrics compacted to higher v_f will show more or less homogenous pressure distributions. Given result variability, it is concluded that heterogeneity and patterns of high compaction pressure zones do vary from fabric to fabric, but without specific relationship to fabric architecture, stacking sequence, surface density, cover factor or v_f . Patterns of high compaction pressure zones vary but their quantitative coverage remains mostly unchanged, Figure 6, with heterogeneity always present.

High compaction pressures were present over approximately 40% of area on average in stacks of dry reinforcements tested in Series 1, generally consistent at all locations A-E but varying between 30% and 45% for different fabric architectures and relative orientations. The results show that heterogeneity in distributions of compaction pressure in stacks of reinforcement fabrics is clearly present and follows clear patterns, with relatively limited differences resulting from nesting. The extent of heterogeneity does vary from fabric to fabric but it cannot be traced to specific macroscopic factors such as fabric architecture, stacking sequence, surface density, cover factor or v_f . Heterogeneity and its effects on further steps of PMC manufacturing operations in processes such as VARTM are clearly fabric dependent. Heterogeneity is also characterised by significant statistical distribution as shown in Figures 5 and 6.

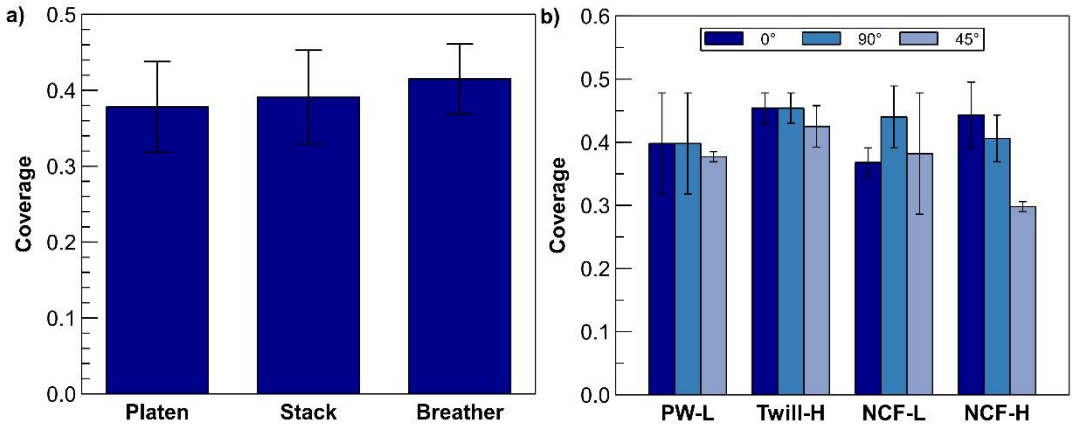

Figure 5: Coverage of high-pressure zones within stacks of fabric plies only; a) at different locations: platen, within stack, release film with breather, b) for different fabric architectures and ply-to-ply relative orientations

Textile Science & Research Journal
ISSN: 3059-846X, Volume – 2, Issue – 2, 2026
DOI: https://doi.org/10.63456/tsrj-2-2-46

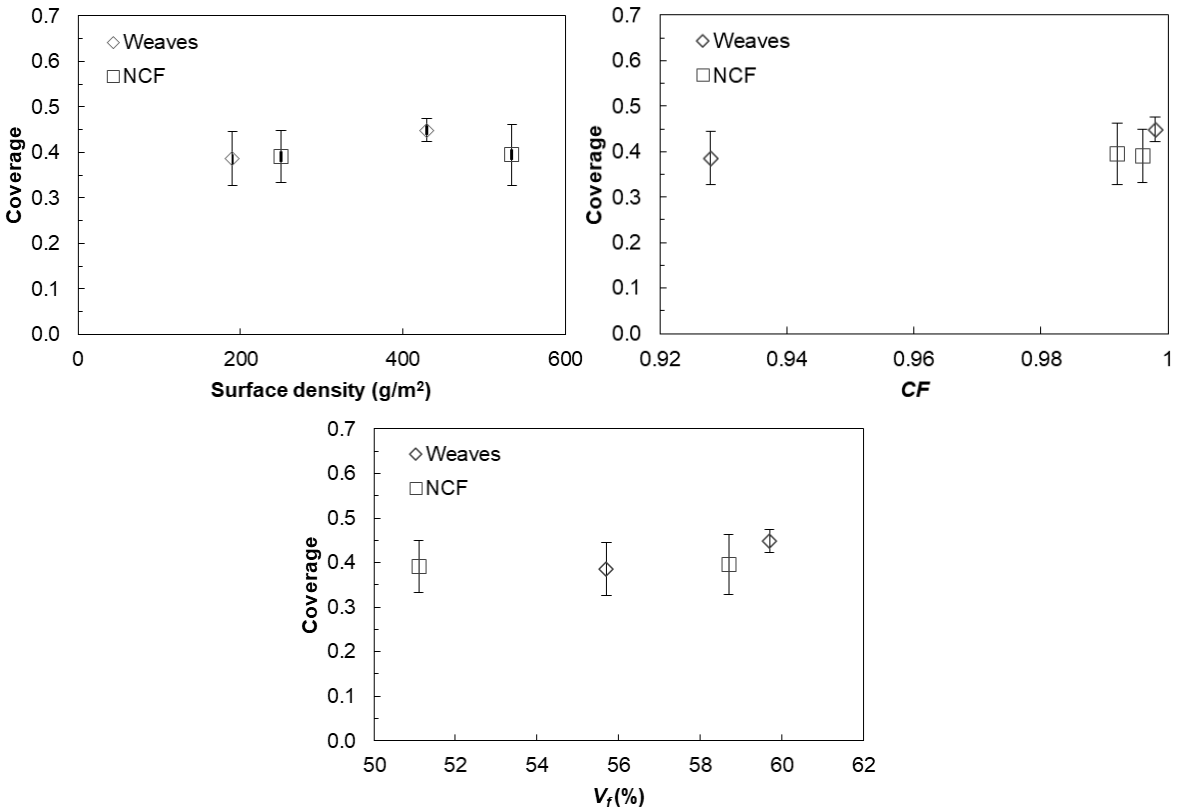

Figure 6: Coverage of high-pressure zones within stacks of fabric plies only as a function of: a) fabric surface density, b) fabric cover factor *CF*, c) fabric V_f under 1.0 bar

3.2 SERIES 2: DISTRIBUTION OF COMPACTION PRESSURE IN STACKS OF FABRIC PLIES INTERLEAVED WITH UNCURED RESIN FILM

Pressure distributions at different stack locations tested in Series 2 are presented in Figure 7. Similarly to Figure 4, pressure measurement films appear in white in Figure 7 with high-pressure zones where compaction pressure exceeded 0.5 bar appearing in red. Again, all pressure measurement films measured 50.4 mm by 25.4 mm, capturing multiple fabric repeating unit cells. At location A, the presence of resin films increases compaction pressure homogeneity in plies next to the platen, with pressure distribution patterns otherwise similar to those observed for stacks of fabrics only tested in Series 1. Regular patters remain clear as a result of yarn and stitch lines crossovers, with no strong effects of nesting. Transitions between zones of higher and lower compaction pressure are more progressive, with zones of higher compaction pressure generally extending further compared to results of test Series 1.

At location B, combined conformability of the resin film, release film and breather leads to even clearer increases in homogeneity of compaction pressure distributions compared with stacks of fabric only tested in Series 1. For most fabrics, yarn or stitch line locations are not readily apparent. The difference in behaviours observed on the platen and release film with breather sides aligns with differences in behaviour observed in stacks of fabrics only tested in Series 1, and the effect is further compounded by the presence of resin film.

Within stacks at locations C, D and E the presence of resin film increases homogeneity of compaction pressure distributions but in each case, clear patterns of high-pressure zones still feature. The effect of stitch lines in NCF fabrics remains but with less prominence over the effect of yarns. Hence, resin film increases pressure distribution uniformity but it does not eliminate repeating patterns.

The results of quantitative analysis of pressure patterns imprinted on all measurement films tested in Series 2 appear in Figures 8 and 9. Results indicate that heterogeneity and patterns for zones of high compaction pressure resulting from fabric architecture largely remain in the presence of highly compliant resin film in the stacks, but they are less pronounced than for stacks of fabric only. This was confirmed quantitatively by markedly greater coverage of high-pressure zones at approximately 55%, Figure 8,

Textile Science & Research Journal
ISSN: 3059-846X, Volume – 2, Issue – 2, 2026
DOI: https://doi.org/10.63456/tsrj-2-2-46

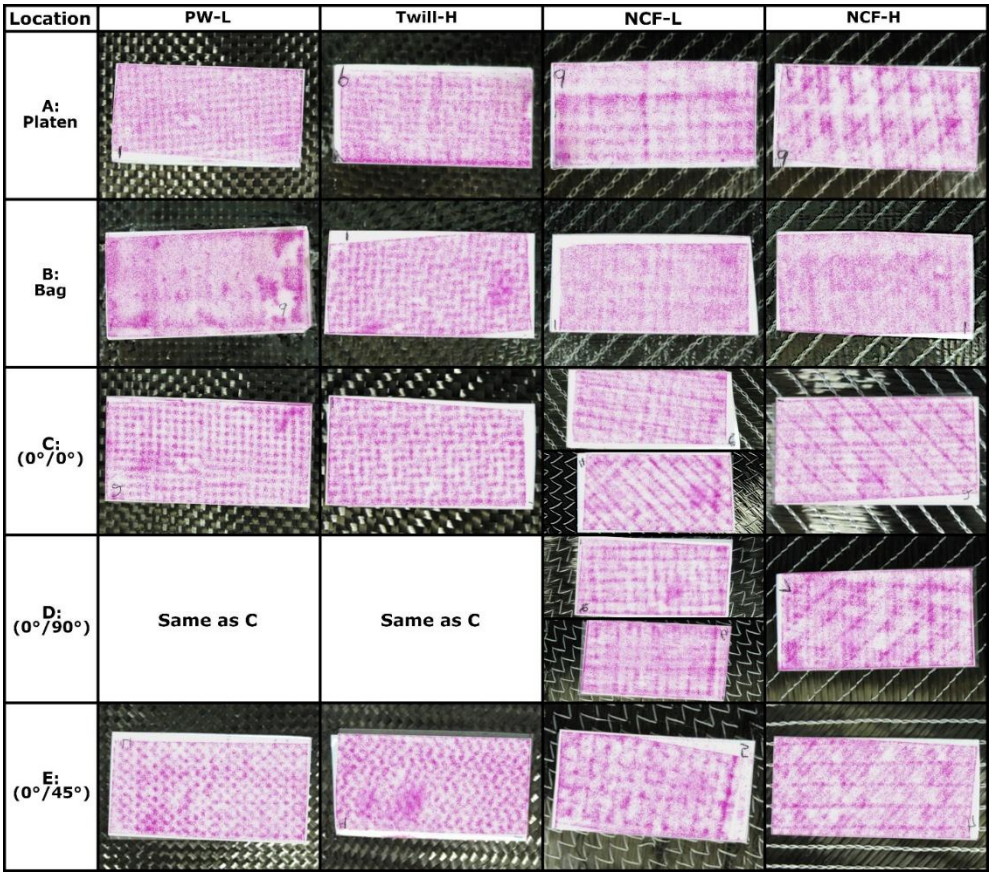

Figure 7: Pressure distribution within stack of PW-L, Twill-H, NCF-L and NCF-H fabrics plies interleaved with uncured resin films, at locations A, B, C, D and E within stacks

compared with approximately 40% for stacks of fabric only, Figure 5. Similarly to observations made for stacks of fabrics only, variation of high-pressure zone coverage is greater between different fabrics than between specific locations, which were not observed in test Series 2, Figure 8. Here again, heterogeneity varies from fabric to fabric but it cannot be traced to specific macroscopic factors such as fabric architecture, stacking sequence, surface density, cover factor or v_f , Figure 9. Resin films used in RFI PMC manufacturing influence the distribution of compaction pressure by dampening the effects of fabric architecture. Nevertheless, heterogeneous distributions of compaction pressure in compacted stacks largely remain.

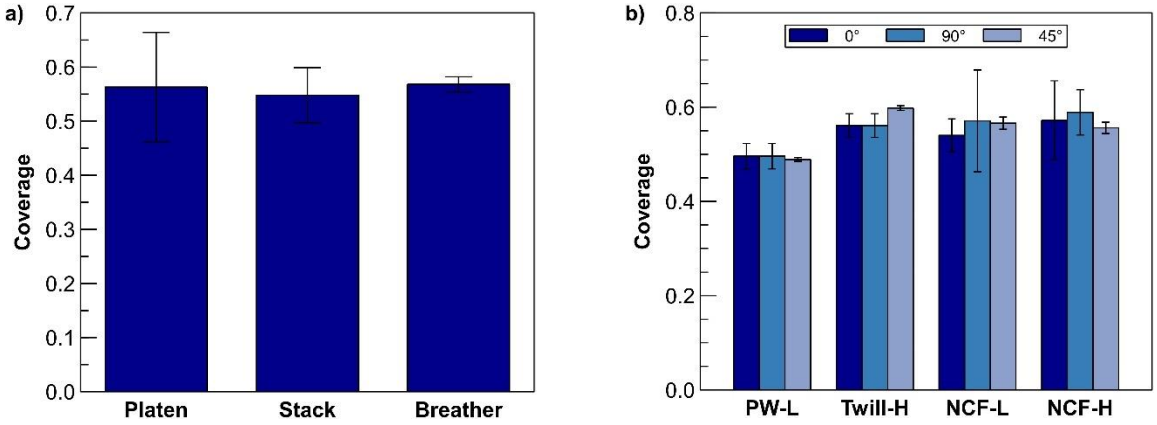

Figure 8: Coverage of high-pressure zones within stacks of fabric plies interleaved with resin films; a) at different locations: platen, within stack, release film with breather, b) for different fabric architectures and ply-to-ply relative orientations

Textile Science & Research Journal
ISSN: 3059-846X, Volume – 2, Issue – 2, 2026
DOI: https://doi.org/10.63456/tsrj-2-2-46

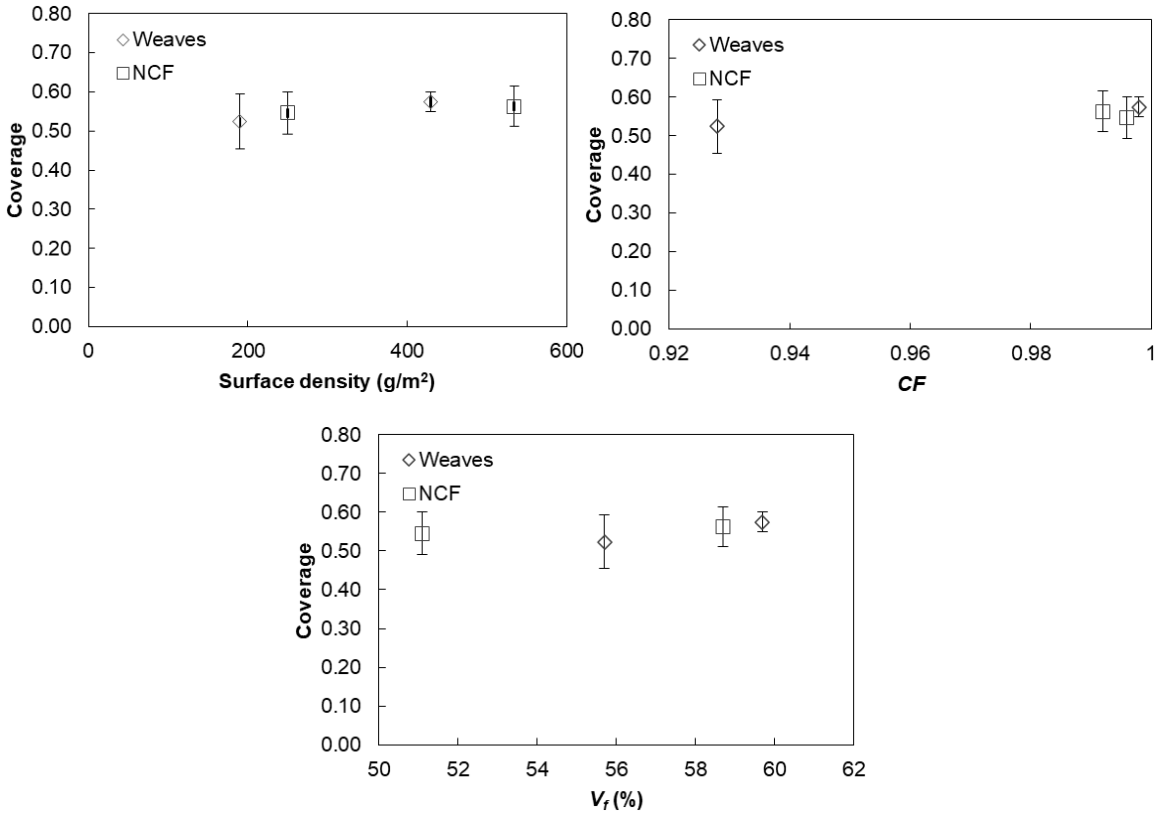

Figure 9: Coverage of high-pressure zones within stacks of fabric plies interleaved with resin films as a function of: a) fabric surface density, b) fabric cover factor *CF*, c) fabric V_f under 1.0 bar

4. DISCUSSION

Pressure measurement films are highly effective for observing and describing the distribution of pressure within stacks of reinforcement fabrics used in PMC manufacturing. Pressure distributions in these stacks are clearly heterogenous with zones of high-pressure forming clear repeating patterns, even in large samples representative of industrial manufacturing and devoid of artificial translational alignment.

Pressure heterogeneity is influenced primarily by the compliance of any nearby resin film or flexible ancillary such as peel ply, breather plies and vacuum film. High compaction pressures were present over 40% of area on average in stacks of dry reinforcements tested in Series 1, and over 55% of area on average in interleaved stacks tested in Series 2, with more progressive transitions between areas of lower and higher compaction pressure in the latter case.

Heterogeneity in local compaction pressure distributions also varied between different fabrics, with high compaction pressures zones varying between 30% and 45% for different fabric architectures and relative orientations in stacks of dry reinforcements tested in Series 1, and between 50% and 60% for different fabric architectures and relative orientations in interleaved stacks tested in Series 2.

No correlations were observed between pressure distribution and macroscopic fabric descriptors such as the cover factor, surface density or v_f.

Considering repeating pressure distribution patterns in Figures 4 and 7, high pressure zones are clearly and closely linked to fabric architecture; they appear at yarn and stitch line crossovers found in individual fabric plies. These locations feature more material in the thickness direction, and thus have lower capability for compaction. It can be conjectured that pressure distribution patterns in fabric stacks may be predicted from a detailed description of fabric architecture. This was confirmed by superposing topographical maps of fabrics obtained by 3D imaging and profilometry using a Keyence VHX 2000 digital optical microscope, Figure 10a. Topographical height values were used for creating normalized intensity maps, Figure 10b, where intensity varied from 0 for lowest height to 1 for greatest height. These maps were subjected to translations and rotations for replicating ply positioning, and the stacking process was modelled by combining the associated intensity maps. Calculations were performed using MATLAB.

Textile Science & Research Journal
ISSN: 3059-846X, Volume – 2, Issue – 2, 2026
DOI: https://doi.org/10.63456/tsrj-2-2-46

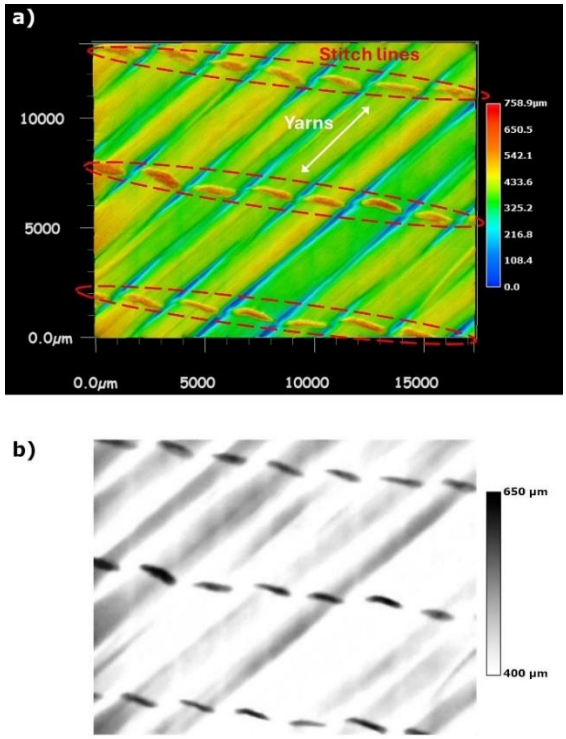

Figure 10: Example of digitalisation process using dry fabric NCF-H: a) raw topographical map of the fabric, and b) intensity map used for geometrical manipulation

Two case studies are presented to validate the hypothesis. These examples were selected to represent both woven and non-crimp fabrics. Patterns of pressure distribution obtained from both pressure measure films and topographical maps are compared for dry fabrics PW-L and NCF-H in Figure 11. Experimental measurements are noisier and show greater redistribution of pressure around stitch lines compared to topographical models, but the models capture all distinct features found in compacted fabric stacks including misalignment, nesting and the effect of ply-to-ply orientation. Considering that the topographical maps are based solely on the surface of a single side of the fabrics, the results strengthen the hypothesis that pressure distribution patterns are affected mostly by pairs of contacting yarns crossovers and/or stiches of contiguous plies, and little from yarns or fabrics away from the contact interface.

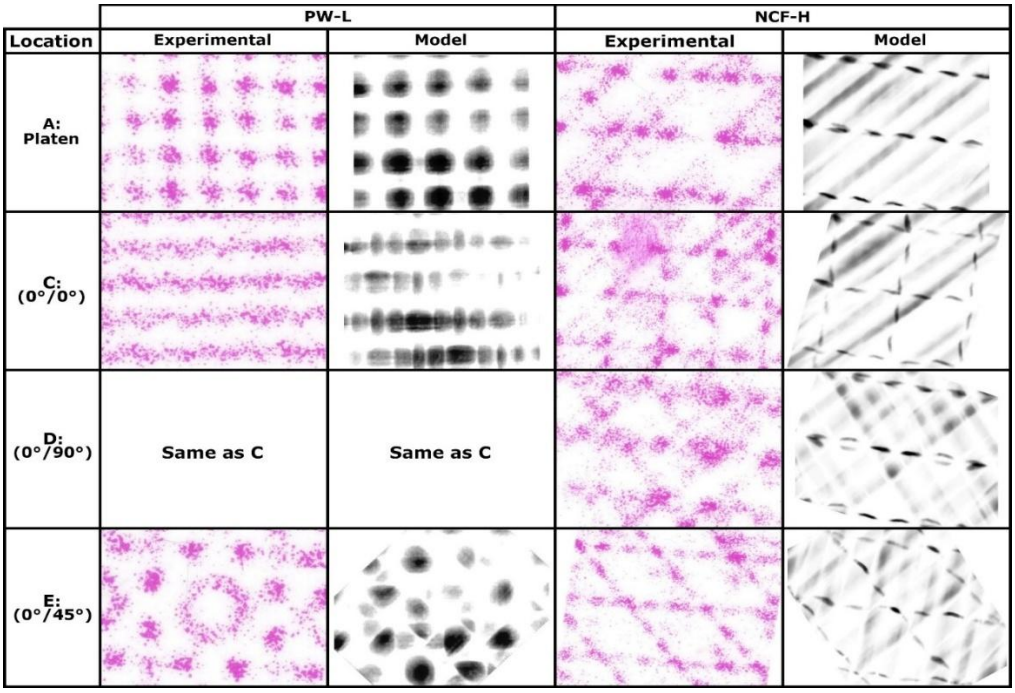

Figure 11: Selected examples comparing experimental and modelled patterns of pressure distribution within PW-L and NCF-H dry fabric stacks

5. CONCLUSION

Stacks of four woven and NCF carbon fibre reinforcement fabrics representative of PMC manufacturing processes such as VARTM, and similar stacks interleaved with films of uncured epoxy resin representative of PMC manufacturing processes such as RFI, were compacted under 1.0 bar nominal pressure. The reinforcement fabrics were characterised by different surface densities and cover factors. Distributions of compaction pressure at different locations within the stacks were measured directly in-situ, and analysed both qualitatively and quantitatively.

Pressure measurement films were highly effective for observing pressure distributions within the stacks. All pressure distributions were clearly heterogeneous, with high pressure zones forming clear repeating patterns.

Pressure heterogeneity was influenced by the compliance of any nearby resin film or flexible ancillary such as peel ply, breather plies or vacuum film, and by fabric architecture. High compaction pressures were present over approximately 40% of area on average in stacks of dry reinforcements tested in Series 1, varying between 30% and 45% for different fabric architectures and relative ply orientations in dry stacks. High compaction pressures were present over approximately 55% of area on average in interleaved stacks tested in Series 2, varying between 50% and 60% for different fabric architectures and relative ply orientations in interleaved stacks. More progressive transitions between areas of lower and higher compaction pressure were observed in interleaved stacks tested in Series 2.

No correlations were observed between pressure distribution heterogeneity and macroscopic fabric descriptors such as the cover factor, surface density or v_f.

Distributions of compaction pressure are clearly related to fabric architecture; zones of higher pressure appear at yarn and stitch line crossovers found in individual fabric plies. Conversely, pressure distribution patterns observed on one side of a fabric ply were largely independent from pressure distribution patterns observed on the other side of the same ply. Effects of nesting were visible on opposing faces of neighbouring plies; however, their effects were not seen to extend beyond these zones of immediate contact. Variable nesting did not preclude the formation of clear repeating patterns of high compaction pressures zones within stacks representative of industrial manufacturing, hence much larger than single textile repeating unit cells and devoid of artificial translational alignment.

REFERENCES

[1] Werlen V, Vocke R, Brauner C, Dransfeld C, Michaud V and Rytka C. A model for the consolidation of hybrid textiles considering air entrapment, dissolution and diffusion. *Composites Part A* 2023; 166: 107413
[2] Rouhi MS, Liu JL, Bin Hamzah MR, Tan VBC and Tay TE. Effects of manufacturing on the structural performance of composites in vacuum assisted resin transfer molding. *J Reinf Plast Compos* 2023; 42(5-6): 264-278
[3] Droste D, Krishnappa L, Bornemann S, Ohlendorf JH, Vargas Gleason MG, Herrmann AS and Lang W. Investigation of the compaction behaviour of a quasi-unidirectional non-crimp fabric during the vacuum infusion process. *J Compos Mater* 2022; 56(16): 2509-2524
[4] Bender M and Fauster E. Experimental characterization of transverse fabric compressibility by means of in-situ-impregnation. In: *Proceedings of the 20th European Conference on Composite Materials: Composites Meet Sustainability,* Lausanne, Switzerland, 26-30 June 2022, 3: 718-725
[5] Ince ME. Numerical analyses on compaction behavior of nonwoven glass fiber fabric. *J Text Inst* 2022; 113(7): 1281-1290
[6] Blößl Y and Schledjewski R. A robust empirical model equation for the compaction response of textile reinforcements. *Polym Compos* 2021; 42(1): 297-308
[7] Kastanis D, Steiner H, Fauster E and Schledjewski R. Compaction behavior of continuous carbon fiber tows: an experimental analysis. *Adv Manuf: Polym Compos Sci* 2015; 1(3): 169–174
[8] Li L, Zhao Y, Yang J, Zhang J and Duan Y. An experimental investigation of compaction behavior of carbon non-crimp fabrics for liquid composite molding. *J Mater Sci* 2015; 50(7): 2960-2972
[9] Cao Z, Zhan L, Ma B, Xie M and Guo J. The key technologies for fiber-reinforced polymer composites manufacturing: A state-of-the-art review. *Thin-Walled Struct* 2025; 217, 113773
[10] Robitaille F and Gauvin R. Compaction of textile reinforcements for composites manufacturing. II: Compaction and relaxation of dry and H2O-saturated woven reinforcements. *Polym Compos* 1998; 19(5): 543-557
[11] Pearce N and Summerscales J. The compressibility of a reinforcement fabric. *Compos Manuf* 1995; 6(1): 15-21
[12] Robitaille F and Gauvin R. Compaction of textile reinforcements for composites manufacturing. III: Reorganization of the fiber network. *Polym Compos* 1999; 20(1): 48-61
[13] Robitaille F and Gauvin R. Compaction of textile reinforcements for composites manufacturing. I: Review of experimental results. *Polym Compos* 1998; 19(2): 198-216
[14] Yong AXH, Aktas A, May D, Endruweit A, Lomov SV, Advani S, Hubert P, Abaimov SG, Abliz D, Akhatov I, Ali MA, Allaoui S, Allen T, Berg DC, Bickerton S, Caglar B, Causse P, Chiminelli A, Comas-Cardona S, Danzi M, Dittmann J, Dransfeld C, Ermanni P, Fauster E, George A, Gillibert J, Govignon Q, Graupner R, Grishaev V, Guilloux A, Kabachi MA, Kelle A, Kind K, Large D, Laspalas M, Lebedev OV, Lizaranzu M, Long AC, López C, Masania K, Michaud V, Middendorf P, Mitschang P, van Oosterom S, Schubnel R, Sharp N, Sousa P, Trochu F,

Umer R, Valette J, Wang JH. Experimental characterisation of textile compaction response: A benchmark exercise. *Composites Part A* 2021; 142: 106243

[15] Yong AXH, Endruweit A, George A, May D, Aksoy YA, Ali MA, Allen T, Bender M, Bodaghi M, Caglar B, Caglar H, Chiminelli A, Comas-Cardona S, de Ribains R, Dittmann J, Dransfeld C, Fauster E, Guilloux A, Hubert P, Idapalapati S, Ivensr J, Janzen J, Jiang Y, Khan T, Laspalas M, LeBel F, Lee J, Liu X, Lizaranzu M, Lomov SV, Lopez C, Masania K, Michaud V, Middendorf P, Miguel S, Narayana SS, Park CH, Ravisankar Padma S, Riffard L, Pingert C, Rougier V, Sas H, Sayinbas D, Sousa P, Sozer M, Steinhardt M, Umerf R, Vincent JD, Werlen V, Yuksel O. Through-thickness compaction response of reinforcement fabrics: Development of a test standard. *Composites Part A* 2026; 200, 109348

[16] Chen B and Chou TW. Compaction of woven-fabric preforms: nesting and multi-layer deformation. *Compos Sci Technol* 2000; 60(12–13): 2223-2231

[17] Yousaf Z, Withers PJ and Potluri P. Compaction, nesting and image based permeability analysis of multi-layer dry preforms by computed tomography (CT). *Compos Struct* 2021; 263: 113676

[18] Stolyarov O, Ershov S. Experimental study and finite element analysis of mechanical behavior of plain weave fabric during deformation through a cross-section observation. *Mater Today Commun* 2022; 31, 103367

[19] Kim J-H, Wang Z-J, Kwon K-E, Shim W-S, Yang S-B and Kwon D-J. Evaluation of resin impregnation using self-sensing of carbon fibers. *Polym Test* 2024; 131, 108331

[20] del Río JS, Ridruejo Á, Martínez V, Jiménez JL, Ramos C, Vilatela JJ and González CD. CNTs monitoring sensors for resin infusion optimization. Sens Actuat A-Phys 2023; 364, 114852

[21] Yu Y, Cui X, Liang Z, Qing X and Yan W. Monitoring of three-dimensional resin flow front using hybrid piezoelectric-fiber sensor network in a liquid composite molding process. *Compos Sci Technol* 2022; 229, 109712

[22] Ali MA, Irfan MS, Khan T, Ubaid F, Liao, K and Umer R. In-situ monitoring of reinforcement compaction response via MXene-coated glass fabric sensors. *Compos Sci Technol* 2022; 227: 109623

[23] Wu W and Li W. A novel material for simulation on compaction behavior of glass fiber non-crimp fabric. *Compos Struct* 2019; 219: 8-16

[24] Kulkarni S, Khan KA, Alhammadi K, Cantwell WJ and Umer R. A visco-hyperelastic approach to model rate dependent compaction response of a 3D woven fabric. *Composites Part A* 2022; 163, 107229

[25] Du W, Shan Z, Liu F, Wu X and Zou G Analysis and modeling of the mechanical behavior of the compaction process of flexible guided 3D weaving. *Polym Compos* 2023; 44(9): 5755-5768

[26] Sun D, Zhang W, Zou J, Xiong Y, Tang C and Zhang W. Coupled 3D non-orthogonal constitutive model for woven composites in preforming and compaction processes. *Manuf Lett* 2024; 41: 412-420